Influence of Different End Region Cooling Arrangements on End-Winding Heat Transfer Coefficients in Electrical Machines

David A. Staton[1] Member
Mircea Popescu[1] Senior Member
Douglas Hawkins[1]
Aldo Boglietti[2] Senior Member
Andrea Cavagnino[2] Senior Member
1) Motor Design Ltd, Ellesmere, Shropshire, SY12 OEG, UK
2) Politecnico di Torino, Dipartimento di Ingegneria Elettrica, 10129 Torino, ITALY
e-mail: mircea.popescu@motor-design.com

***Abstract* – In this paper the influence of the end-winding heat transfer on the thermal analysis of induction motors is presented. Experimental tests on two induction motor configurations - Open Drip Proof (ODP) and Total Enclosed Fan Cooled (TEFC) frames – are performed and the heat transfer coefficients are determined and validated in a lumped thermal analysis network. The cooling effect of the wafters present in the induction motor cage end-rings is also discussed.**

Keywords: **induction motors, thermal model, parameter identification, end-winding cooling, heat transfer coefficients**

I. Introduction

Thermal analysis of electric motors is in general regarded as a more challenging area of analysis than electromagnetic analysis in terms of the ease of constructing a model and achieving good accuracy. This is due to the fact that many electric motor electromagnetic problems can be reduced to a 2-dimensional problem which can be fully described using a simple set of analytical equations, or Maxwell's equations when using numerical finite-element analysis [9,11]. The thermal analysis of an electric motor is seen to be more of a 3-dimensional problem, with complex heat transfer phenomena to solve such as heat transfer through complex composite components like the wound slot, temperature drop across interfaces between components and complex turbulent air flow within the end-caps around the end-winding that includes rotational effects. Based on experimental data, thermal lumped equivalent networks may be successfully used to predict the temperature rise in any part of the machine [3-8], [10],[12-17].

II. Thermal Problems in Induction Motors

Due to the large number of thermal exchanges simultaneously active, the thermal phenomena inside an electrical motor are very complex. Conduction, natural convection, forced convection and radiation are all present with a relative weight that depends on the motor cooling system (natural convection, fan cooling, water cooling, and so on). In addition, many heat sources are active at the same time. As a consequence, it is not easy to split the causes and effects in thermal exchange phenomena. The most widely used procedure to analyze these heat transfer exchanges is the definition of thermal networks based on lumped parameters as shown in a rich technical literature on this topic (see references list in [1-2]). A difficult aspect of this approach is the correct determination of heat transfer coefficients and the resulting thermal resistances for convection and radiation heat transfer. When using an experimental approach to help quantify heat transfer coefficients, the use of a standard motor is often not the best choice, in particular when a single thermal effect has to be analyzed [12], [13]. In fact, in complex systems, the thermal phenomena analysis can be simplified where, as far as possible, the heat sources can be separately activated. In particular, when the stator winding cooling effects are under analysis, it is convenient that only the stator joule losses should be present and the other thermal sources should not be active. Obviously, this condition is particularly true when the phenomena involved in the end-winding cooling have to be studied [6]. As a consequence, in the proposed approach, suitable induction motor prototypes have been built [6], [10].

III. Experimental Data

Two prototypes have been built and tested to analyze different end-winding cooling arrangements. The first prototype is a standard 2 poles Total Enclosed Fan Cooled (TEFC) motor (generically defined as Motor A), while the second one is a 4 poles Open Drip Proof (ODP) motor (generically defined as Motor B). For increasing the cooling effects of the end-windings, some openings are present in the main frame and in the two end-caps of this motor. Since only the inner cooling effect on the end-winding must be active, the external fan of Motor A has been removed.

For both prototypes the rotor laminations and the rotor squirrel cages have been totally replaced by a nylon cylinder, as shown in Fig.1. In order to maintain the internal ventilation effect, the two end rings of the original rotors have been fixed by screws on the two sides of the plastic cylinder, as seen in Fig. 2.

TABLE I
NAME PLATE DATA OF THE PROTOTYPES

Motor #	Motor A	Motor B
Enclosure type	TEFC	ODP
Frequency, [Hz]	60	60
Rated Voltage, [V]	230/460	230/460
Rated current, [A]	8.0/4.0	13.4/6.7
Pole number	2	4
Rated speed, [rpm]	3530	1760
Rated efficiency, [%]	88.5	87.5
Endwinding over-length, [mm] *	48	45
Endwinding perimeter, [mm] **	108	90
Endwinding average diameter [mm]	145	150

* Over length from the lamination of a single endwinding in axial direction
** Perimeter of the endwinding cross section

The plastic rotor diameter has the same value as the original one. The rated data of the two prototypes are reported in Table I. Fig. 3 shows the TEFC Motor A on the left side and the ODP Motor B in the right side. In the bigger rotor (Motor B), very long end ring wafters are adopted (as evident in Fig.1) to improve the end-windings ventilation. Conversely, the smaller rotor (Motor A) has regular end ring wafters, as usually adopted in this machine type.

The two motors are not monitored by thermal sensors, but the winding temperatures is estimated from rise in phase resistance value while the stator lamination temperature can be measured by a digital thermometer through a hole available inside the terminal box for both the motors. Due to the plastic rotors, the two motors cannot rotate by themselves, so the two rotors are mechanically connected to an industrial TEFC induction motor (generically called “Drive Motor”) using the mechanical output shafts of this machine. In particular, the regular output shaft is connected to one motor under test while the shaft on the other side is connected to the second prototype removing the external fan and cowling of the Drive Motor. In Fig.4, the complete test bench is shown. The two motors under test have both been connected to the Drive Motor because this configuration allows performing the thermal tests on the two machines at the same time, halving the number of tests. In order to introduce a high thermal resistance between the three shafts, the two mechanical joints have been realized using a simple rubber water-pipe. This joint does not present problems because only a very small torque, due to the mechanical losses, is involved. In addition, the rubber water-pipe joints introduce a thermal disconnection, reducing the thermal flux from one motor to the other. As a consequence, the three motors can be considered thermally decoupled. This configuration minimizes the ventilation effects on the prototype endcaps that could be introduced by traditional mechanical joints.

In order to increase the thermal decoupling, a plastic barrier is introduced between the Drive Motor and Motor A, as shown in Fig.4. The aim of the plastic barrier is to stop the air flow produced by Motor B versus Motor A.

Fig.1: Prototype plastic rotors
(Motor A lower and Motor B upper).

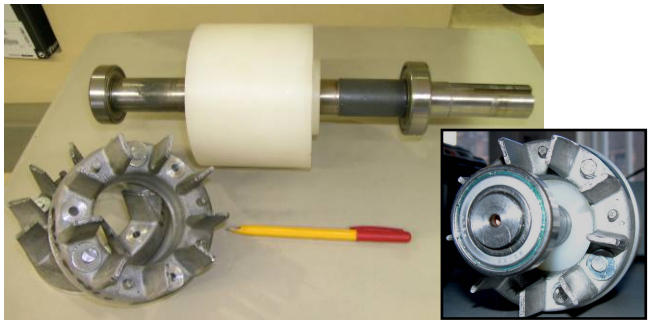

Fig.2: End ring positioning on the plastic rotor.

Fig. 3: TEFC Motor A (left) and ODP Motor B (right).

Fig. 4: Test bench with the two motors under test
(Motor B in TEFC configuration)

An inverter is used to supply the Drive Motor, in order to impose the requested speed to the two plastic rotors. The test

bench has been positioned in a room with ambient temperature variation lower than 2 °C throughout the day. The test rig has been position on a wood support to reduce the thermal exchange through the motor feet.

Using the previously described test bench the following tests have been performed on each prototype:

- Thermal test with a DC supply connecting the three windings in series and with the rotor still. This test is the reference condition for the thermal models set up.
- Thermal test with a DC supply connecting the three windings in series and with the rotor running at constant speed imposed by the Drive Motor. In particular the following mechanical speeds have been considered: 250, 500, 750, 1000, 1500, 2000, and 2500 rpm.

Several experimental tests have been performed in order to investigate and quantify the influence of different cooling arrangements on the end-winding – motor frame thermal exchanges. In particular, in order to provide evidence of the cooling effects due to the enclosure type, Motor B has been tested both in ODP configuration and in TEFC configuration (closing all the frame and end caps openings with a plastic tape, Fig.4). Also, in order to provide evidence of the cooling effects due to the end ring wafters, both Motor A and motor B in TEFC configuration have been tested with end rings mounted on the plastic cylinder and without end rings fixed on the plastic cylinder.

It is important to remark that removing the end rings from the plastic cylinder would drastically reduce the inner ventilation effects.

The use of a DC supply involves stator joule losses only, simplifying the thermal analysis. In fact, with a sinusoidal supply, the loss contribution values are not known accurately and the loss separation is made following international standards. In DC supply conditions the thermal system is more obvious and an easier thermal analysis can be adopted. In addition, knowing the winding resistance at a reference temperature, with a DC supply the ratio between the voltage and current allows continuous monitoring of the winding temperature during the temperature test.

In order to avoid motor damage, the DC supply voltage for the two motors has been chosen to inject an appropriate constant DC power of 100 W for Motor A and 150 W for Motor B. These powers lead to an increased temperature rise (about 70-80 °C for both prototypes) compatible with the motor insulation class. It is important to remember that during the tests the prototypes are without any type of external ventilation.

In the tests, the stator winding, stator lamination and external motor frame temperatures have been measured in thermal steady state condition, together with the ambient temperature. The external motor frame temperature is the average values of 25 measured temperatures on the main frame and on the end caps, as described in [10].

IV. Thermal Models

The two prototypes are modeled in a lumped thermal network model [18]. This included the nylon rotor and fixed values of stator copper losses for the two motors. Based on the geometrical dimensions and material properties (Figs. 5-6), equivalent thermal resistances corresponding to the conduction heat transfer are calculated. The convection heat transfer is modeled via thermal resistances calculated using best available correlations in the literature.

The heat transfer coefficient for all surfaces within the endcaps is calculated using Schubert's expression which is detailed in [19]:

$$h = 15 \cdot \left[1 + (0.4v)^{0.9} \right] \quad (1)$$

It has a natural convection term and a forced convection component that is a function of the peripheral air velocity (v in m/s).

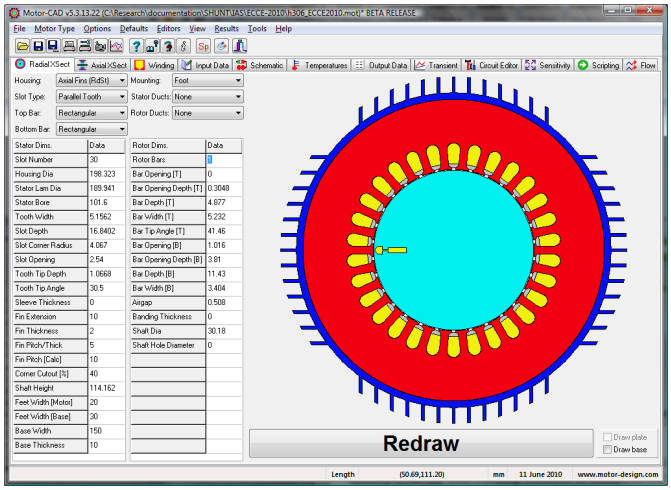

(a)

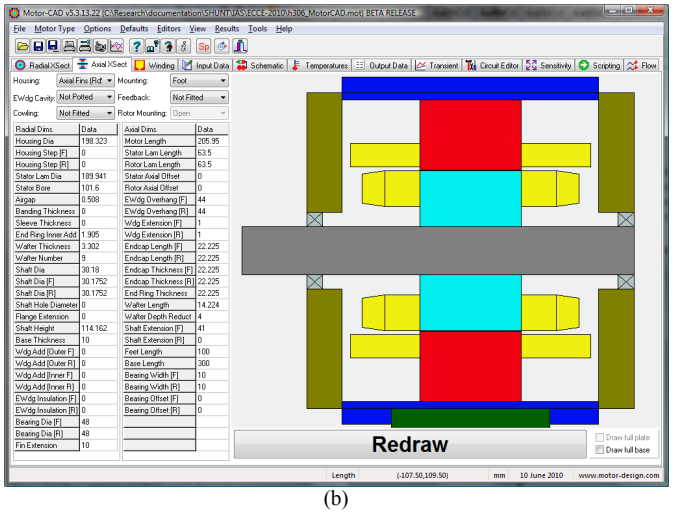

(b)

Fig. 5 Cross-section (a) and axial view (b) of Motor A in thermal model

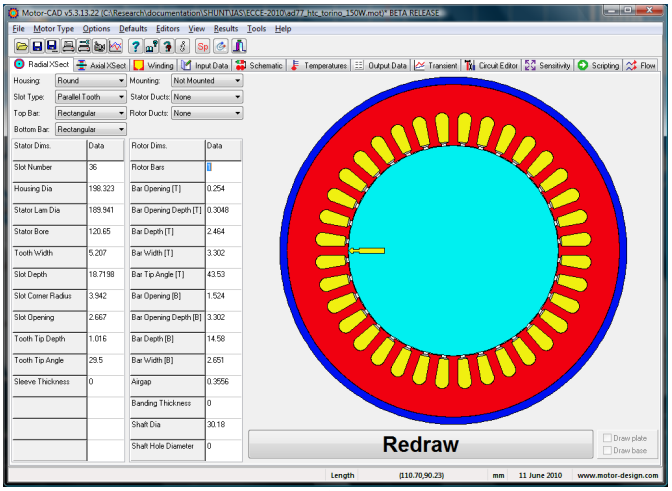

(a)

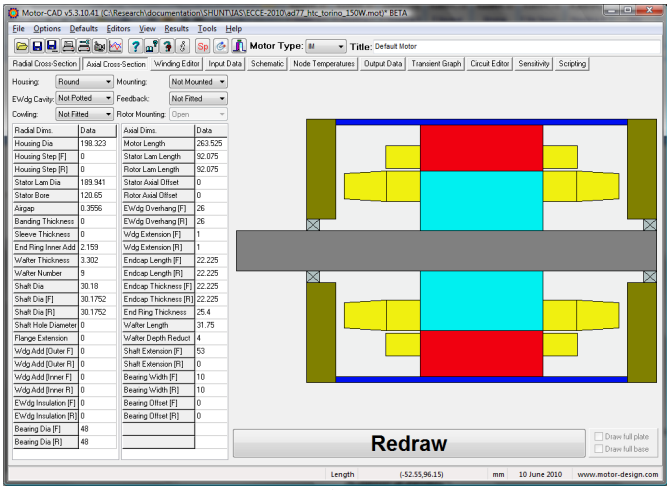

(b)

Fig. 6 Cross-section (a) and axial view (b) of Motor A in thermal model

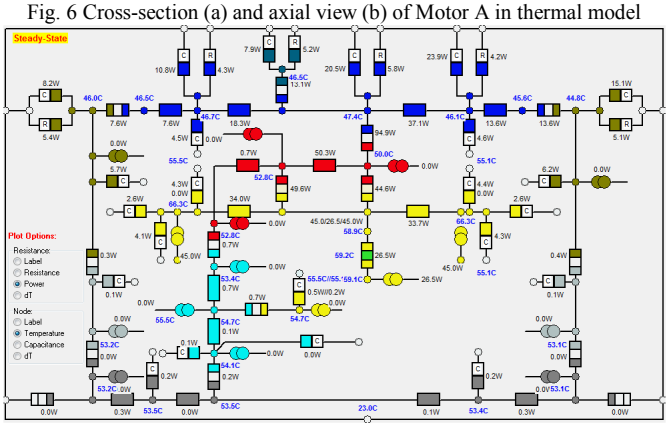

Fig. 7 Thermal network for Motor A

Figs. 7 and 8 show the equivalent thermal network for Motor A and Motor B respectively. As expected the hottest point in each motor under the specific DC tests is the end-winding.

In a TEFC configuration as in motor A the local air velocity over the end-winding surfaces is related to the rotor peripheral velocity which is a function of the rotational speed.

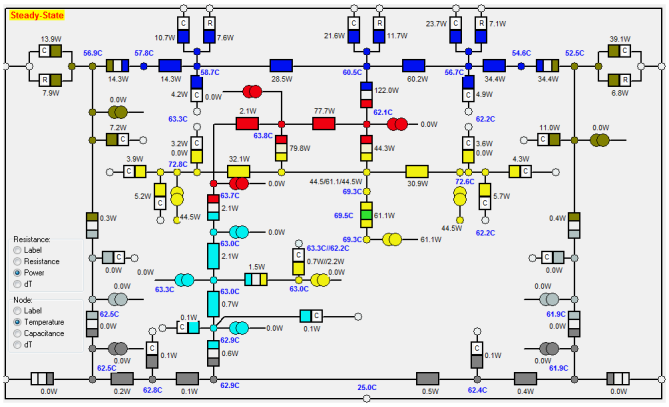

Fig. 8 Thermal network for Motor B

End-Winding Fanning Factor (Fig. 10) is used to relate the magnitude of rotational air velocity in the end-caps to the rotor peripheral velocity. If the internal fan is large the internal air velocity will be close to the rotor peripheral velocity and the end-winding fanning factor is 1. If there is no internal fan and the ends of the rotor are smooth the internal air velocity will be much less and the end-winding fanning factor will be closer to 0. Values of end-winding fanning factor equal to 0.8 and 1.0 were used for motors A and B respectively. A larger value was used for motor B as it has larger wafters incorporated into the rotor end rings.

A small amount of heat transfer is due to the radiation and both prototypes have painted surfaces with an emissivity factor of 0.9.

V. Discussions

A. TEFC Motor Results

Fig. 9 shows the stator winding, stator iron and motor frame steady state temperature rise versus the rotor speed for Motor A. The small rise in temperature of the motor frame at high speed is due to the increase of the bearing mechanical losses and the increase of the ventilation losses inside the closed end caps. Since this loss contribution is small and it cannot be measured with the used test bench, it has been neglected.

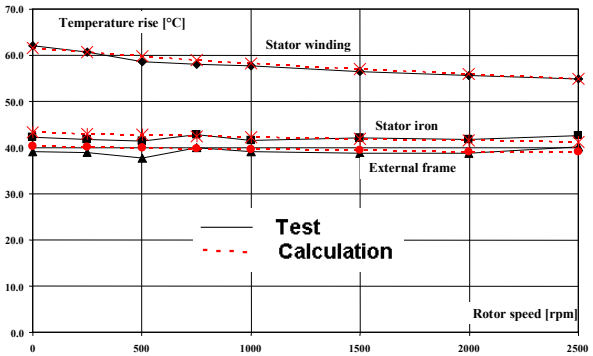

Fig. 9 Predicted and measured winding, stator lamination and frame temperature rise versus the rotor speed (Motor A)

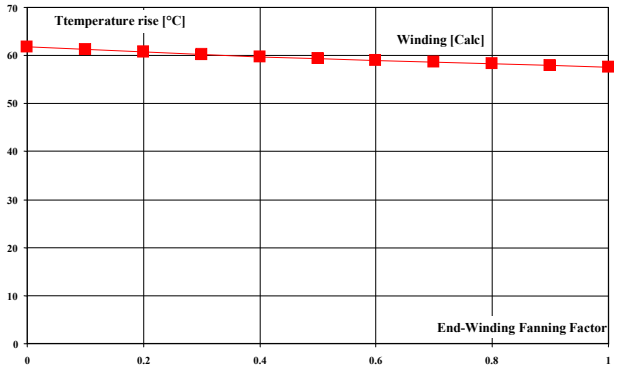

Fig. 10 Motor A winding temperature rise versus the selection of the end winding fanning factor

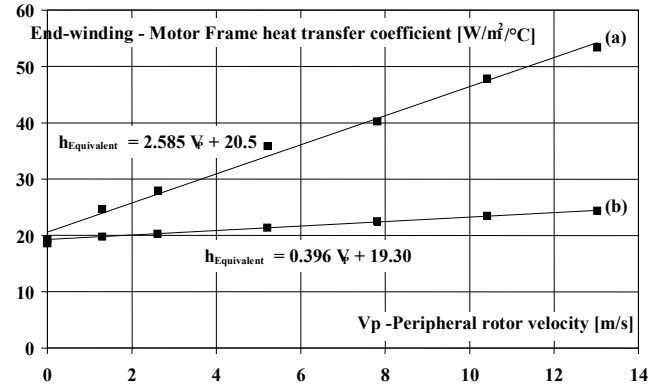

Fig. 11 End-winding – motor frame equivalent heat transfer coefficient for the Motor A: (a) with end rings, (b) without end rings.

The heat transfer coefficients between the end-winding and the motor frame have been evaluated as reported in [10]. The obtained results are shown in Fig.11 where the equivalent (taking into account natural convection, radiation and forced convection phenomena in the inner air end regions) heat transfer coefficients as function of the peripheral rotor velocity are reported.

One can note the essential role of the end-ring wafters in increasing the end-winding – frame heat transfer coefficient. For this specific example the peripheral rotor velocity corresponding to the motor rated speed is around 10m/s. The heat transfer coefficient will increase from 24W/m^2/^{0}C to 48 W/m^2/^{0}C when the end-ring wafters are present.

B. ODP Motor Results

Motor B was tested in three different conditions. In the figures concerning this machine three letters are used to identify the test type:

(a) Motor B with open frame openings and with end rings (original ODP configuration, Fig.3),

(b) Motor B with closed frame openings, TEFC, (Fig.4) and with end rings positioned on the plastic rotor (Fig.1)

(c) Motor B with the frame openings closed, TEFC, (Fig.4) and the end rings removed by the plastic cylinder (Fig.2).

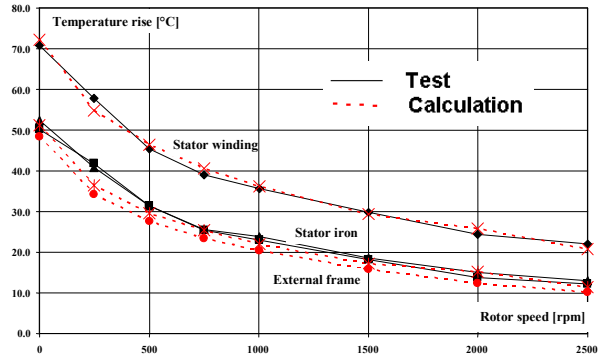

Fig. 12 Predicted and measured winding, stator lamination and frame temperature rise versus the rotor speed (Motor B – ODP configuration)

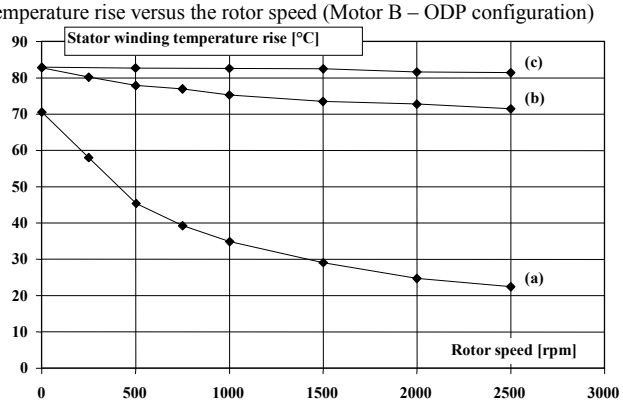

Fig. 13 Measured stator winding temperature rise for the Motor B: (a) ODP, (b) TEFC, (c) TEFC without end rings.

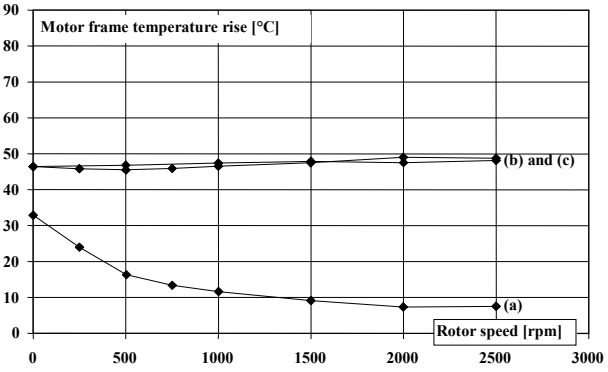

Fig. 14 Measured motor frame temperature rise for the Motor B: (a) ODP, (b) TEFC, (c) TEFC without end rings.

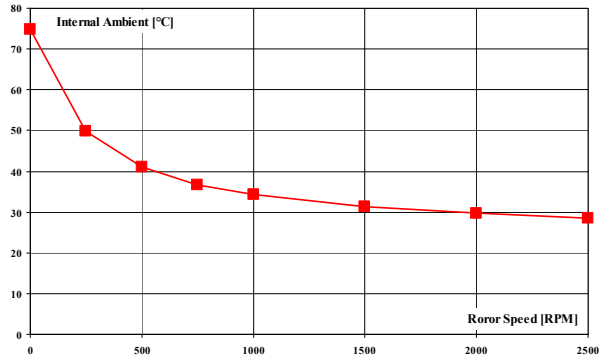

Fig. 15 Predicted internal ambient as a function of rotor speed for Motor B (ODP configuration)

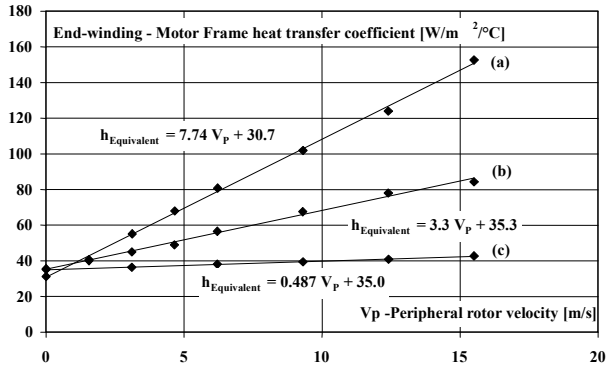

Fig. 16 End-winding – motor frame equivalent heat transfer coefficient for the Motor B: (a) ODP, (b) TEFC, (c) TEFC without end rings.

Fig. 12 shows the stator winding, stator iron and motor frame steady state temperature rise versus the rotor speed for Motor B. There is an important temperature drop when the rotor speed is increasing, i.e. from 70°C to 20°C temperature rise in the stator winding when rotor speed increases from standstill to 2500rpm.

The effects of the changing from ODP to TEFC enclosure type are shown in Fig.13 and Fig.14, where the measured stator winding and motor frame temperatures are reported as a function of the rotational speed. It is interesting to observe that with the rotor at standstill and TEFC configuration, both the stator winding and the motor frame temperature increase with approximately 12°C with respect to the original frame configuration. This is explained by the fact that certain amount of air enters end-caps even at zero speed leading to a reduction in air temperature.

Motor B in ODP configuration has opening in the end-caps. These openings have two major cooling effects which are taken account of in the thermal model:

- The effect of the external air entering the machine reducing the internal ambient. The amount of air entering the machine is proportional to the rotational speed according to fan scaling laws. In this case the fan forcing air into the machine is attached to the rotor by way of wafters on the end rings. The predicted internal air temperature in the machine as a function of rotational speed is shown in Fig 15.
- The increase in air velocity over end winding and internal surfaces of the end-caps and housing due to air entering the machine. The local velocity over a surface is a function of the air entering the machine and the rotational velocity.

The ODP motor is more complex to model accurately than the TEFC machine as it is necessary to estimate the volume flow rate entering the machine at one rotor speed. The volume flow rate at other speed is calculated assuming flow is proportional to speed as indicated by fan scaling laws.

The equivalent heat transfer coefficient as a function of the peripheral rotor velocity is shown in Fig. 16.

Similar to the case of Motor A, one can note the essential role of the end-ring wafters in increasing the end-winding – frame heat transfer coefficient. For Motor B the peripheral rotor velocity corresponding to the motor rated speed is around 6m/s.

C. Forced Heat Transfer Coefficients

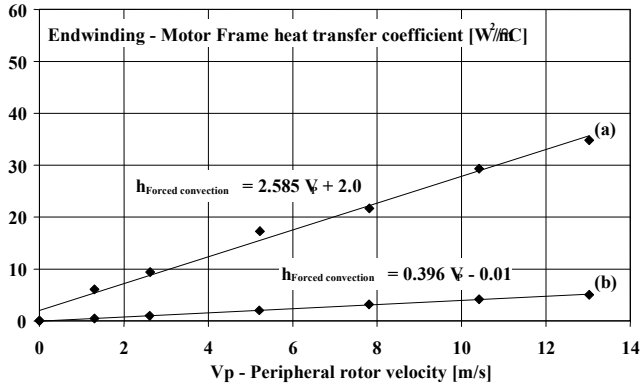

Fig. 17 Estimated end-winding – motor frame forced convection heat transfer coefficient for the Motor A: (a) with end rings, (b) without end rings.

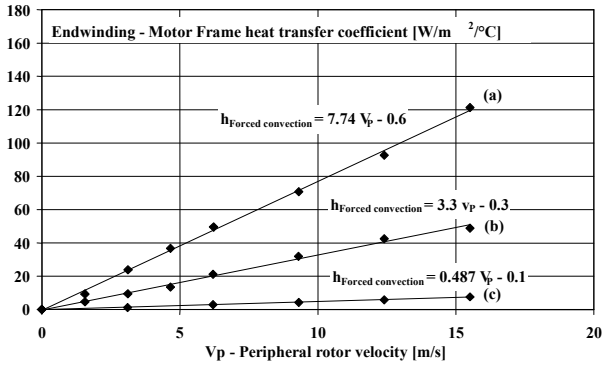

Fig. 18 Estimated end-winding – motor frame forced convection heat transfer coefficient for the Motor B: (a) ODP, (b) TEFC, (c) TEFC without end rings.

Figs. 17 and 18 show the estimated values of the forced convection heat transfer coefficients for Motor A and Motor B respectively.

Comparing the results in Fig.18 it is important to observe that the heat transfer coefficient values for the (c) case (Motor B in TEFC configuration without the end rings) are practically equal to the values estimated for Motor A without the end rings (line (b) in Fig.17) and they are practically negligible.

The slope of the regression line for Motor B in TEFC configuration with end rings (line (b) in Fig. 18) is slightly steeper than the slope of the regression line for Motor A with end rings (line (a) in Fig.17). This result is coherent with the presence of longer end-ring wafters for motor B, as shown in Fig.1. Also, the ODP configuration leads to a considerable increase in the forced convection heat transfer coefficient as compared to TEFC configuration, i.e. 120W/m^2/^{0}C vs. 48 W/m^2/^{0}C.

C. Literature Result Comparison

The heat transfer phenomena in the end region of TEFC induction motors have been subject of several studies, which proposed the use of the following general formulation for the related equivalent heat transfer coefficient:

$$h = k_1 \cdot \left[1 + k_1 \cdot v^{k_3}\right] \quad (2)$$

Where: k_1, k_2 and k_3 are curve fit coefficients, and v is the peripheral air velocity for the surface under consideration [13]-[17].

Previously published data are in the region delimited by the two continuous curves reported in Fig.19. The same figure shows the position of the obtained equivalent end-winding - motor frame heat transfer coefficients for Motor A and Motor B in TEFC configuration. There is good agreement between the results obtained and those from literature.

Another more detailed comparison is given in Fig. 20, where the estimated equivalent heat transfer coefficient for Motor A (TEFC) is plotted together with various expressions available in the literature. The thermal model described in Section IV is using the Shubert (EW) variation of the heat transfer coefficient with peripheral air velocity.

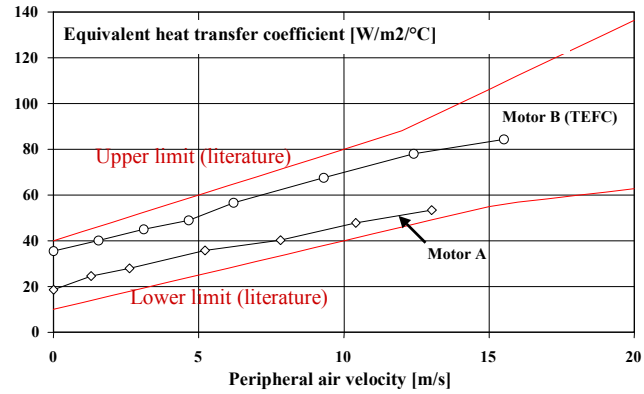

Fig. 19 Comparison between the obtained equivalent convection heat transfer coefficients for the two prototypes (TEFC configuration) and the upper and lower limit values reported in literature.

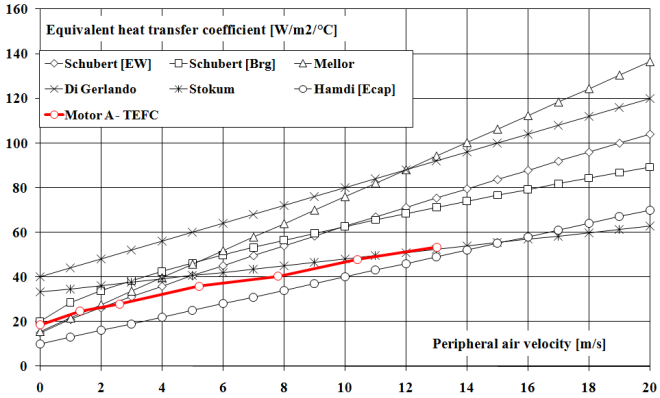

Fig. 20 Comparison between the obtained equivalent convection heat transfer coefficients for the Motor A and the values reported in literature.

We can observe a very good correlation with estimated values. The heat transfer coefficient tests have some uncertainty due to the estimation of end-windings and end space air cooling temperature and due to the split between active and end-winding cooling ratio. Given these uncertainties, a good agreement between measured and estimated temperatures is achieved for the whole rotor speed range.

VI. Conclusions

This paper presents the effect of different cooling arrangements for induction motor end-windings. In particular, the impact of the frame openings and of the rotor end-ring wafters on the end-winding cooling is analyzed and quantified by means of two prototypes with specially made nylon rotors. The measured temperature rise is used to estimate the heat transfer coefficients concerning the thermal transfer between end-windings and external frame, with respect to the considered cooling arrangements. Measured results are compared with calculated results via thermal networks. A satisfactory agreement test data versus calculated data may be obtained by using a heat transfer coefficient available in the literature, i.e. Schubert equation. The reported results confirm the reliability of the proposed experimental approach and allow the calculation of the equivalent or forced convection heat transfer coefficients to be used in electrical motor thermal networks.

Acknowledgments

The authors would like to thank Alan Barker, Steve Ruffing and Alan Crapo of Emerson Motors, St. Louis, USA, for the support of this project. The authors would also like to acknowledge the support from Prof. TJE Miller, *SPEED* Consortium, Glasgow, UK.

References

[1] A. Boglietti, Guest Editorial of the Special Section on thermal Issues in Electrical machines and drives, *Trans. on Industrial Electronics*, Vol. 55, No. 10, October 2008, pp.3498-3499.

[2] A. Boglietti, A. Cavagnino, D. Staton, M. Shanel, M. Mueller, C. Mejuto "Evolution and Modern Approaches for Thermal Analysis of Electrical Machines", *Trans. on Industrial Electronics*, Vol. 56, No. 3, March 2009, pp.871-882.

[3] A. Boglietti, A. Cavagnino, M. Lazzari, and M. Pastorelli, "A simplified thermal model for variable-speed self-cooled industrial induction motor," *Trans. on Industry Applications*, vol. 39, no. 4, Jul./Aug. 2003, pp. 945–952.

[4] N. Jaljal, J.-F. Trigeol, P. Lagonotte, "Reduced Thermal Model of an Induction Machine for Real-Time Thermal Monitoring", *Trans. on Industrial Electronics*, Vol. 55, No. 10, October 2008, pp.3535-3542.

[5] C. Kral, A. Haumer, T. Bauml, "Thermal Model and Behavior of a Totally-Enclosed-Water-Cooled Squirrel-Cage Induction Machine for Traction Applications", *Trans. on Industrial Electronics*, Vol. 55, No. 10, October 2008, pp.3555-3564.

[6] A. Boglietti, A. Cavagnino, "Analysis of the Endwinding Cooling Effects in TEFC Induction Motors", *Transactions on Industry Applications*, Vol. 43, No. 5, Sept.-Oct. 2007, pp.1214 – 1222.

[7] A. Boglietti, A. Cavagnino, M. Parvis, A. Vallan, "Evaluation of radiation thermal resistances in industrial motors", *Trans. on Industry Applications*, Vol. 42, No. 3, May/June 2006, pp. 688-693.

[8] J. Mugglestone, S.J. Pickering, D. Lampard, "Effect of Geometry Changes on the Flow and Heat Transfer in the End Region of a TEFC Induction Motor", *9th IEE Intl. Conf. Electrical Machines & Drives*, Canterbury, UK, Sept 1999.

[9] C. Micallef, S.J. Pickering, K.A. Simmons, K.J. Bradley, "An Alternative Cooling Arrangement for the End Region of a Totally Enclosed Fan Cooled (TEFC) Induction Motor", *IEE Conf. Rec. PEMD* 08, 3-5 April 2008, York, UK.

[10] A. Boglietti, A. Cavagnino, D. Staton, M. Popescu, C. Cossar, M.I. McGilp, "End Space Heat Transfer Coefficient Determination for Different Induction Motor Enclosure Types", *Trans. on Industry Applications*, Vol. 45, No. 3, May/June 2009, pp. 929-937.

[11] C. Micallef, S. J. Pickering, K. A. Simmons, K. J. Bradley, "Improved Cooling in the End Region of a Strip-Wound Totally Enclosed Fan-Cooled Induction Electric Machine", *Trans. on Industrial Electronics*, Vol. 55, No. 10, October 2008, pp.3517-3524.

[12] M.A Valenzuela, J.A. Tapia, "Heat Transfer and Thermal Design of Finned Frames for TEFC Variable-Speed Motors", *Trans. on Industrial Electronics*, Vol. 55, No. 10, October 2008, pp.3500-3508.

[13] D. A. Staton, A. Cavagnino, "Convection Heat Transfer and Flow Calculations Suitable for Electric Machines Thermal Models", *Trans. on Industrial Electronics*, Vol. 55, No. 10, October 2008, pp.3509-3516.

[14] A. DiGerlando, I. Vistoli, "Thermal networks of induction motors for steady state and transient operation analysis," *Conf. Rec. ICEM*, Paris, France, 1994.

[15] E. Schubert, "Heat transfer coefficients at end winding and bearing covers of enclosed asynchronous machines," *Elektrie*, vol. 22, Apr.1968.

[16] G. Stokum, "Use of the results of the four-heat run method of induction motors for determining thermal resistance," *Elektrotechnika*, vol. 62, no. 6, 1969.

[17] E. S. Hamdi, "*Design of Small Electrical Machines*", New York, Wiley, 1994.

[18] D.A. Staton and D. Hawkins, "*Motor-CAD v5.1 Manual*", Motor Design Ltd., Ellesmere, UK, 2009

[19] D.A. Staton, A. Boglietti, A. Cavagnino, "Solving the More Difficult Aspects of Electric Motor Thermal Analysis, in small and medium size industrial induction motors", *IEEE Transaction on Energy Conversion*, Vol.20, n.3 pp.620-628.